# THE PROPER MOTION VS REDSHIFT RELATION FOR SUPERLUMINAL RADIO SOURCES

BERT W. RUST

*National Bureau of Standards, Gaithersburg, MD, U.S.A.*

STEPHEN G. NASH

*George Mason University, Virginia, U.S.A.*

and

BARRY J. GELDZAHLER

*Applied Research Corporation*

(Received 18 August, 1988)

**Abstract.** Two models for superluminal radio sources predict sharp lower bounds for the apparent velocities of separation. The light echo model predicts a minimum velocity $v_{\min} = 2c$, and the dipole field model predicts $v_{\min} = 4.446c$. Yahil (1979) has suggested that, if either of these models is correct, then $v_{\min}$ provides a 'standard velocity' which can be used to determine the cosmological parameters $H$ and $q_0$. This is accomplished by estimating a lower envelope for the proper motion vs redshift relation. Yahil also argued that the procedure could easily be generalized to include a nonzero cosmical constant $\Lambda$. We derive the formulas relating the proper motion $\dot{\theta}$ to the redshift $z$ in a Friedmann universe with a nonzero $\Lambda$. We show that the determination of a lower envelope for a given sample of measured points $(z_i, \dot{\theta}_i)$ yields an estimate of the angle of inclination $\phi_i$ for each source in the sample. We formulate the estimation of the lower envelope as a constrained maximum likelihood problem with the constraints specified by the expected value of the largest order statistic for the estimated $\phi_i$. We solve this problem numerically using an off-the-shelf nonlinearly constrained nonlinear optimization program from the NAg library. Assuming $\Lambda = 0$, we apply the estimation procedure to a sample of 27 sources with measured values $(z_i, \dot{\theta}_i)$, using both the light echo and the dipole field models. The fits give $H = 103$ km s$^{-1}$ Mpc$^{-1}$ for the light echo model and $H = 46$ km s$^{-1}$ Mpc$^{-1}$ for the dipole field model. In both cases the fits give $q_0 = 0.4$, but the uncertainty in this result is too large to rule out the possibility that $q_0 > 0.5$. When $\Lambda$ is allowed to be a free parameter, we obtain $H = 105$ km s$^{-1}$ Mpc$^{-1}$ for the light echo model and $H = 47$ km s$^{-1}$ Mpc$^{-1}$ for the dipole field model. In both cases the fits give $q_0 = -1$ and $\Lambda/H_0^2 = 6.7$, but no significance can be attached to these results because of the paucity of measured data at higher redshifts. For all of the fits, we compute the corresponding estimates of the $\phi_i$ and compare the cumulative distribution of these values with that expected from a sample of randomly oriented sources. In all cases we find a large excess of sources at low-inclination angles (high apparent velocities). The expected selection effect would produce such an excess, but the excess is large enough to suggest a strong contamination of the sample by relativistic beam sources which would only be seen at low inclination angles.

## 1. Introduction

Although the relativistic beaming model first proposed by Rees (1966) is the most generally accepted explanation for the superluminal radio sources, two other models, which predict lower bounds for the apparent linear velocities of separation, cannot yet be ruled out as an explanation for some or all of these sources. The light echo model, suggested by Lynden-Bell (1977), predicts a minimum velocity $v_{\min} = 2c$, and the dipole field model, suggested by Sanders (1974) and corrected by Milgrom and Bahcall (1978),

*Astrophysics Space Science* **152** (1989) 141–170.

predicts $v_{\min} = 4.446c$. There are, to be sure, difficulties with these two models, but there are also difficulties with the beaming models. The latter have received much more attention from the theoreticians, but De Waard (1986) has suggested some new variants of the light echo model and Scheuer (1984) has proposed new variants of the dipole field model which predict superluminal expansion. There are currently approximately 30 measured angular expansion velocities which are thought to indicate superluminal motion. One does not have to search far in the history of astronomy to find instances where a sample of objects initially thought to be all of the same type turned out to be composed of two or more very different populations. The results of the present study indicate that the superluminal radio sources may constitute a mixed sample of relativistic beam soruces and either light echo or dipole field sources.

The light echo and dipole field models have interesting cosmological implications which follow from their predictions of a minimum apparent velocity of separation. Yahil (1979) suggested that, if either of these models is correct, then the minimum velocity provides a 'standard velocity' which can be used to determine the cosmological parameters $H_0$ and $q_0$ from the proper motion vs redshift relation for the sources. For a Friedmann universe with zero-cosmological constant, that relation can be written as

$$\dot{\theta} = \frac{v_T}{c} \frac{H_0 q_0^2 (1+z)}{q_0 z + (q_0 - 1)(-1 + \sqrt{2q_0 z + 1})},$$

where $z$ is the observed redshift; $\dot{\theta}$, the observed angular velocity of separation, measured in milliarcsseconds per year [mas yr$^{-1}$]; $v_T$, the transverse component of the apparent linear velocity; and $H_0$ and $q_0$, the Hubble parameter and the deceleration parameter. Note that the units of $H_0$ in the above expression are not the ones usually associated with the Hubble constant. We will use $H$ to denote the Hubble constant expressed in [km s$^{-1}$ Mpc$^{-1}$], so that

$$H = 4740.62 H_0 \quad (\text{km s}^{-1}\ \text{Mpc}^{-1}).$$

Yahil's idea was to substitute $v_{\min}$ for $v_T$ and then to determine $H_0$ and $q_0$ so that the above expression defines a lower envelope for the measured $(z, \dot{\theta})$ points.

At the time Yahil made this suggestion, angular separation rates $\dot{\theta}$ had been measured for only 4 superluminal sources. In order to demonstrate the effectiveness of his proposed procedure, he generated a hypothetical data set containing 20 sources with expansion velocities distributed according to the dipole field model in a Friedmann universe with $H = 50$ km s$^{-1}$ Mpc$^{-1}$, $q_0 = 0.5$, and $\Lambda = 0$. The redshifts for the sources were distributed in the interval $0 < z < 1$. Figure 1 shows a plot of these simulated data and the lower envelope generated by the formula

$$\dot{\theta}(z) = 4.446 \frac{(0.0105471)(0.5)^2 (1+z)}{(0.5)z + (-0.5)(-1 + \sqrt{z+1})}.$$

Yahil used this hypothetical data set together with statistical arguments to show that a real data set of the same size should determine $q_0$ to an accuracy $\Delta q_0 \sim 0.1$. He also

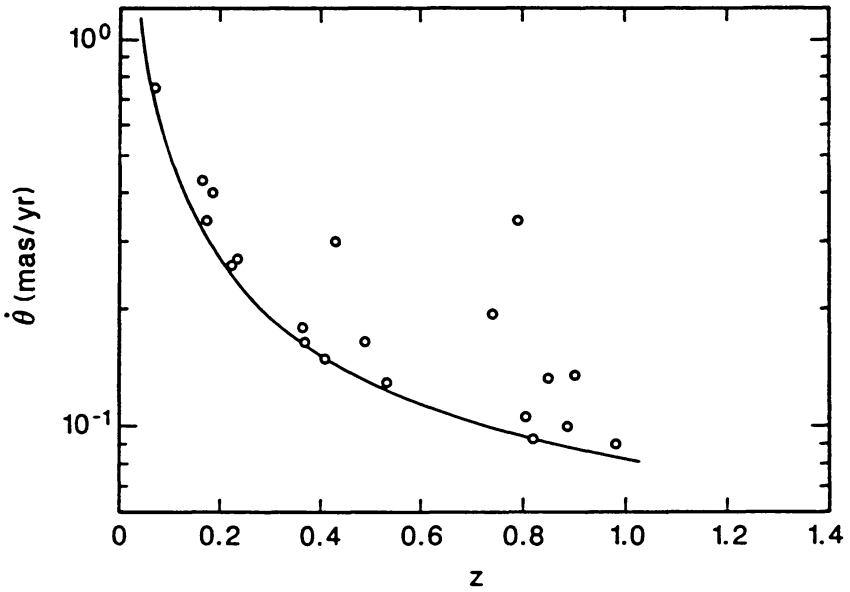


Fig. 1. Yahil's simulated data set and the lower envelope function used to generate it.

argued that the procedure could easily be generalized to include a nonzero cosmological constant $\Lambda$.

In this paper we analyze the proper motion vs redshift relation for a data set recently compiled by Zensus and Pearson (1988). In Section 2 we derive the formulae for the proper motion vs redshift relation in a Friedmann universe with a nonzero cosmological constant. The formulas obtained are valid no matter what the nature of the sources. In Section 3 we show that a determination of the lower envelope function gives estimates of the inclination angles for all of the sources in the sample. These estimates provide a test of the hypothesis that the sources are randomly oriented in space. In this section we also develop a constrained maximum likelihood estimation procedure for determining the required lower envelope function. The numerical methods used to solve the resulting nonlinearly constrained nonlinear estimation problem are described in Section 4. Section 5 describes the validation of the statistical and numerical procedures by applying them to Yahil's simulated data set. The real data are collected in Section 6 and the analysis is applied to them in Section 7. The lower envelope is determined for both the case where the cosmological constant is assumed to be zero and the case where it is taken to be a free parameter in the fit. In both cases, the values obtained for $H$ and $q_0$ are consistent with those obtained by other methods with the light echo model favouring $H \approx 100$ (km s$^{-1}$ Mpc$^{-1}$) and the dipole field model favoring $H \approx 50$ (km s$^{-1}$ Mpc$^{-1}$). In neither case, however, is the distribution of estimated inclination angles consistent with that expected from a single population of randomly oriented sources. The results of this analysis are discussed in Section 8.

## 2. Theory

In a uniform model universe, spacetime has a Robertson–Walker metric,

$$ds^2 = c^2\,dt^2 - R^2(t)\left\{\frac{dr^2}{1-kr^2} + r^2(d\theta^2 + \sin^2\theta\,d\varphi^2)\right\}, \tag{1}$$

where the scale factor $R(t)$ is an arbitrary function of time, independent of the coordinates $(r, \theta, \varphi)$, and the space-curvature constant $k$ is defined by

$$k = \begin{cases} +1\,, & \text{for spherical space}\,, \\ 0\,, & \text{for flat space}\,, \\ -1\,, & \text{for hyperbolic space}\,. \end{cases} \tag{2}$$

Light emitted at time $t_1$ by a source at radial distance $r_1$ and observed at later time $t_0$, at $r = 0$, suffers a redshift (blueshift) given by

$$z = \frac{R(t_0)}{R(t_1)} - 1 = \frac{R_0}{R_1} - 1\,, \tag{3}$$

and the time lapse $\delta t_1$ between events at the distant source produces an observed time lapse

$$\delta t_0 = \frac{R(t_0)}{R(t_1)}\,\delta t_1 = \frac{R_0}{R_1}\,\delta t_1\,. \tag{4}$$

The distance $r_1$ is an unobservable *coordinate distance* which does not change with time even in an expanding model universe. The coordinates $(r, \theta, \varphi)$ form a *comoving* system which expands (or contracts) with the underlying substratum. The present study uses *proper motion distance* $d_M$ which is related to coordinate distance by

$$d_M = R(t_0)r_1 = R_0 r_1\,, \tag{5}$$

(see Weinberg, 1972; Chapter 14, Section 4). If $v_T$ represents the transverse component of the separation velocity for the radio sources in the present study, then the observed angular rate of separation is given by

$$\dot{\theta} = \frac{v_T}{d_M} = \frac{v_T}{R_0 r_1}\,. \tag{6}$$

Since light rays travel along null geodesics, if follows from Equation (1) that light traveling radially to an observer at $r = 0$ from a source at coordinate distance $r_1$ satisfies

$$c\int_{t_1}^{t_0}\frac{dt}{R(t)} = \int_0^{r_1}\frac{dr}{\sqrt{1-kr^2}} = \begin{cases} \sin^{-1} r_1\,, & k = +1\,; \\ r_1\,, & k = 0\,; \\ \sinh^{-1} r_1\,, & k = -1\,. \end{cases} \tag{7}$$

If the function $I(t)$ is defined by

$$I(t) = \int_{t}^{t_0} \frac{\mathrm{d}t}{R(t)} = \int_{R(t)}^{R_0} \frac{\mathrm{d}R}{R\dot{R}} \; ;$$

or, equivalently,

$$I(R(t)) = \frac{1}{R_0} \int_{(R(t)/R_0)}^{1} \frac{1}{(R/R_0)} \frac{1}{(\dot{R}/R_0)} \, d\left(\frac{R}{R_0}\right),$$

then, by (3),

$$I(R_1) = \frac{1}{R_0} \int_{(1+z)^{-1}}^{1} \frac{1}{(R/R_0)} \frac{1}{(\dot{R}/R_0)} \, d\left(\frac{R}{R_0}\right). \tag{8}$$

Thus, if Equation (7) is 'solved' for $r_1$ and the result is substituted into (6), then the angular rate of separation can be written

$$\dot{\theta} = \begin{cases} \dfrac{v_T}{R_0 \sin[cI(R_1)]} \, , & k = +1 \, , \\ \dfrac{v_T}{R_o cI(R_1)} \, , & k = 0 \, , \\ \dfrac{v_T}{R_0 \sinh[cI(R_1)]} \, , & k = -1 \, . \end{cases} \tag{9}$$

Equation (9) is strictly a kinematic result, valid for arbitrary scale functions $R(t)$. To get an equation suitable for comparison with observations, it is necessary to restrict the class of allowed scale functions by specifying the dynamics of the model universe. The dynamics most often used for this purpose is General Relativity. In a Robertson–Walker universe, Einstein's gravitational field equations become

$$8\pi G\rho = \frac{3}{R^2} (kc^2 + \dot{R}^2) - \Lambda \, , \tag{10}$$

$$\frac{8\pi G}{c^2} p = -\frac{2\ddot{R}}{R} - \frac{\dot{R}^2}{R^2} - \frac{kc^2}{R^2} + \Lambda \, , \tag{11}$$

where $\rho$ and $p$ are the (uniform) density and pressure, respectively, and $\Lambda$ is the cosmological constant (see McVittie, 1965, Chapter 8, Section 2). Multiplying

Equation (10) by $R^3$ and differentiating with respect to $t$ on both sides gives

$$8\pi G \frac{\mathrm{d}}{\mathrm{d}t}(\rho R^3) = 3R^2\dot{R}\left[\frac{2\ddot{R}}{R} + \frac{\dot{R}^2}{R^2} + \frac{kc^2}{R^2} - \Lambda\right],$$

whence, by (11),

$$\frac{\mathrm{d}}{\mathrm{d}t}(\rho R^3) = -\frac{p}{c^2}(3R^2\dot{R}),$$

or

$$\frac{\mathrm{d}}{\mathrm{d}t}(\rho R^3) + \frac{p}{c^2}\frac{\mathrm{d}}{\mathrm{d}t}(R^3) = 0, \tag{12}$$

which is an expression of the energy conservation principle. It is usually assumed that $p = 0$ so this relation gives

$$\rho = \rho_0\left(\frac{R_0}{R}\right)^3, \tag{13}$$

where $\rho_0$ and $R_0$ are the values of $\rho$ and $R$ at the time of observation.

Using the $p = 0$ assumption in Equation (11) gives, for the epoch of observation,

$$\frac{kc^2}{R_0^2} = -\frac{2\ddot{R}_0}{R_0} - \frac{\dot{R}_0^2}{R_0^2} + \Lambda. \tag{14}$$

The second term on the right-hand side is just the negative of the square of the Hubble parameter

$$H_0 = \frac{\dot{R}_0}{R_0},$$

and the first term can be rewritten as

$$-\frac{2\ddot{R}_0}{R_0} = -2H_0^2\ddot{R}_0\frac{R_0}{\dot{R}_0^2} = 2H_0^2 q_0,$$

where $q_0$ is the deceleration parameter (see McVittie, 1965, Chapter 8, Section 3). Making these substitutions in Equation (14) we obtain

$$\frac{kc^2}{R_0^2} = (2q_0 - 1)H_0^2 + \Lambda. \tag{15}$$

Similarly, for the epoch of observation, Equation (10) becomes

$$\frac{8\pi G}{3}\rho_0 = \frac{kc^2}{R_0^2} + H_0^2 - \frac{1}{3}\Lambda,$$

whence, by (15),

$$\frac{8\pi G}{3}\rho_0 = 2q_0H_0^2 + \frac{2}{3}\Lambda\,. \tag{16}$$

Now, if Equation (10) is divided by $R_0^2$, it can be rewritten to give

$$\left(\frac{\dot{R}}{R_0}\right)^2 = -\frac{kc^2}{R_0^2} + \left(\frac{8\pi G}{3}\rho + \frac{1}{3}\Lambda\right)\left(\frac{R}{R_0}\right)^2,$$

which, by Equations (13), (15), and (16), gives

$$\left(\frac{\dot{R}}{R_0}\right)^2 = \frac{\Lambda}{3}\left(\frac{R}{R_0}\right)^2 + [(1-2q_0)H_0^2 - \Lambda] + 2\left[q_0H_0^2 + \frac{\Lambda}{3}\right]\frac{1}{(R/R_0)}\,.$$

Using this expression allows us to rewrite the integrand of Equation (8),

$$\frac{R_0}{R}\frac{R_0}{\dot{R}} = \left\{\frac{\Lambda}{3}\frac{R^4}{R_0^4} + [(1-2q_0)H_0^2 - \Lambda]\frac{R^2}{R_0^2} + 2\left[q_0H_0^2 + \frac{\Lambda}{3}\right]\frac{R}{R_0}\right\}^{-1/2},$$

and substituting the dummy variable $\xi$ for $(R/R_0)$ gives

$$I(R_1) = \frac{1}{R_0}\int_{(1+z)^{-1}}^{1}\left\{\frac{\Lambda}{3}\xi^4 + [(1-2q_0)H_0^2 - \Lambda]\xi^2 + \right.$$

$$\left. + 2\left[q_0H_0^2 + \frac{\Lambda}{3}\right]\xi\right\}^{-1/2} \mathrm{d}\xi\,. \tag{17}$$

Now by Equation (15),

$$\frac{k}{R_0^2} = \frac{1}{c^2}[\Lambda - H_0^2(1-2q_0)]\,,$$

from which it follows that

$$k = +1 \Leftrightarrow \Lambda > H_0^2(1-2q_0)\,, \quad \frac{1}{R_0} = \frac{1}{c}\sqrt{\Lambda - H_0^2(1-2q_0)}\,,$$

$$k = 0 \quad \Leftrightarrow \Lambda = H_0^2(1-2q_0)\,, \tag{18}$$

$$k = -1 \Leftrightarrow \Lambda < H_0^2(1-2q_0)\,, \quad \frac{1}{R_0} = \frac{1}{c}\sqrt{H_0^2(1-2q_0) - \Lambda}\,.$$

Substituting this result into Equations (9) and (17) allows us to write

$$\dot{\theta} = \frac{v_T}{c}\,Q(z;\Lambda,H_0,q_0)\,, \tag{19}$$

where,

$$Q(z;\Lambda,H_0,q_0)=\begin{cases}\dfrac{\sqrt{\Lambda-H_0^2(1-2q_0)}}{\sin[I(z;\Lambda,H_0,q_0)\sqrt{\Lambda-H_0^2(1-2q_0)}]}\,, & \Lambda>H_0^2(1-2q_0)\,,\\[2ex] \dfrac{1}{I(z;\Lambda,H_0,q_0)}\,, & \Lambda=H_0^2(1-2q_0)\,,\\[2ex] \dfrac{\sqrt{H_0^2(1-2q_0)-\Lambda}}{\sinh[I(z;\Lambda,H_0,q_0)\sqrt{H_0^2(1-2q_0)-\Lambda}]}\,, & \Lambda<H_0^2(1-2q_0)\,,\end{cases} \tag{20}$$

with,

$$I(z;\Lambda,H_0,q_0)=\int_{(1+z)^{-1}}^{1}\left\{\frac{\Lambda}{3}\,\xi^4+[(1-2q_0)H_0^2-\Lambda]\xi^2+2\left[q_0H_0^2+\frac{\Lambda}{3}\right]\xi\right\}^{-1/2}\mathrm{d}\xi\,. \tag{21}$$

These expressions define $\dot{\theta}$ in terms of the observable $z$ and the three parameters $\Lambda$, $H_0$, and $q_0$ which must be determined by fitting. They also depend on the unobservable $v_T/c$, but both the light echo model and the dipole field model predict a strict lower bound for this quantity:

$$\text{light echo model} \;\Rightarrow\; \min\left\{\frac{v_T}{c}\right\}=2.0\,,$$

$$\text{dipole field model} \;\Rightarrow\; \min\left\{\frac{v_T}{c}\right\}=4.446\,.$$

Thus the strategy will be to fit a lower envelope to the observed $\dot{\theta}$ vs $z$ relation. The functional form for the lower envelope is

$$\dot{\theta}_{\min}(z;\Lambda,H_0,q_0)=\frac{v_{\min}}{c}\,Q(z;\Lambda,H_0,q_0)\,, \tag{22}$$

where

$$v_{\min}=\begin{cases}2.0c\,, & \text{light echo model}\,,\\ 4.446c\,, & \text{dipole field model}\,.\end{cases} \tag{23}$$

The usual practice in cosmological studies is to assume that $\Lambda=0$. In this special case, $q_0$ cannot be negative, and Equation (22) reduces to

$$\dot{\theta}_{\min}(z;H_0,q_0)=\frac{v_{\min}}{c}\,\frac{H_0q_0^2(1+z)}{q_0z+(q_0-1)(-1+\sqrt{2q_0z+1})}\,, \tag{24}$$

which is the expression given by most authors (e.g., Weinberg, 1972, Chapter 15).

## 3. Statistics

For both the light echo model and the dipole field model, determining the lower envelope function, $\dot{\theta}_{\min}(z; \Lambda, H_0, q_0)$, gives an estimate of the angle of inclination for each of the radio sources in the sample. In both cases the lower envelope corresponds to the inclination $\pi/2$, and for the measured data points $(z_i, \dot{\theta}_i)$, the distance above the envelope varies inversely with the inclination angle.

The situation for the light echo model is represented in Figure 2 which is taken from Lynden-Bell (1977). The illuminated tube is inclined with an angle $\phi$ with respect to the line-of-sight, so the apparent velocity of separation becomes

$$v_T = v_T(\phi) = \frac{2c}{\sin\phi} = \frac{v_{\min}}{\sin\phi}\,, \tag{25}$$

which is minimized when $\phi$ is a right angle. From Equation (19) if follows that, if $\Lambda \neq 0$,

$$\phi = \sin^{-1}\left[\frac{v_{\min}}{c}\,\frac{Q(z; \Lambda, H_0, q_0)}{\dot{\theta}}\right], \tag{26}$$

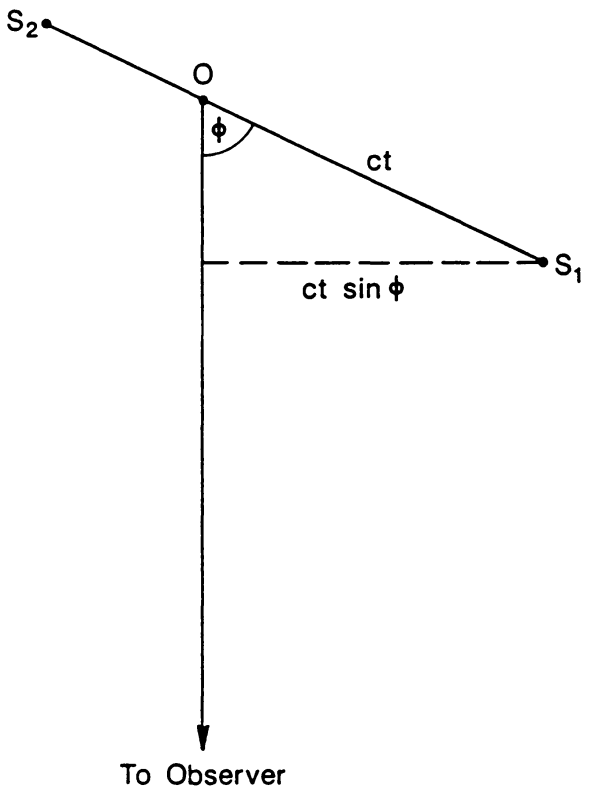


Fig. 2. A flash at $O$ in a tube illuminates two patches of plasma seen by the observer at time $t$ after the initial burst would have been observed. Because of the time delay effect, the illuminated patches at positions $S_1$ and $S_2$ appear to be seprating faster than the speed of light.

where $Q(z; \Lambda, H_0, q_0)$ is given by Equation (20). For the special case $\Lambda = 0$, this reduces to

$$\phi = \sin^{-1}\left[\frac{v_{\min}}{c}\,\frac{H_0 q_0^2(1+z)}{q_0 z + (q_0 - 1)\left(-1 + \sqrt{2q_0 z + 1}\right)}\,\frac{1}{\dot{\theta}}\right]. \tag{27}$$

An assumption that the plasma tubes are oriented randomly in space means that, if the lower envelope function is known, the measured data points $(z_i, \dot{\theta}_i)$, $i = 1, 2, \ldots, m$ define a random sample $\phi_1, \phi_2, \ldots, \phi_m$ chosen from the probability density distribution

$$f(\phi) = \sin(\phi), \qquad 0 \le \phi \le \frac{\pi}{2}. \tag{28}$$

The cumulative density function for this distribution is

$$F(\phi) = 1 - \cos(\phi), \qquad 0 \le \phi \le \frac{\pi}{2}. \tag{29}$$

Our strategy will be to: (1) fit the lower envelope, (2) compute the corresponding sample $\phi_1, \phi_2, \ldots, \phi_m$ and construct its cumulative distribution, and (3) check whether that distribution is well approximated by Equation (29).

The situation for the dipole field model is similar, with $\phi$ being the angle between the observer's line-of-sight and the symmetry axis of the dipole. This is illustrated in Figure 3

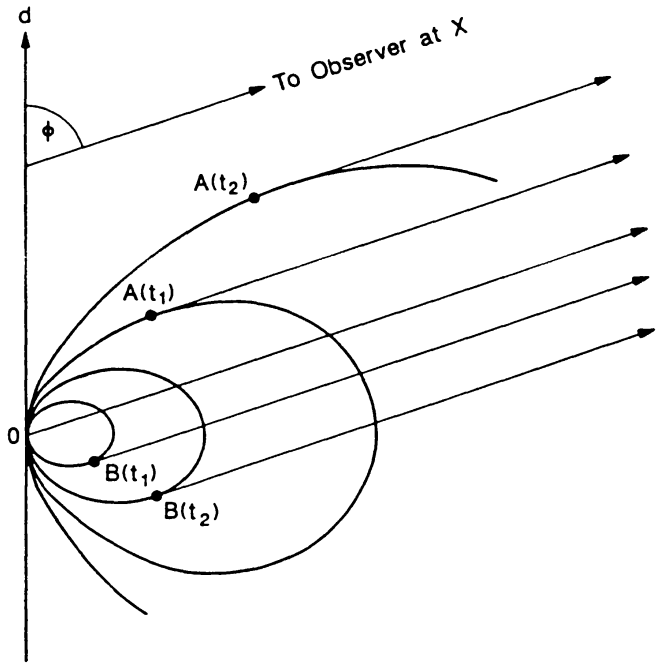


Fig. 3. Charged particles ejected at $O$ move relativistically along the field lines, emitting radiation tangentially. A distant observer sees only radiation from a plane defined by the dipole axis $d$ and his line-of-sight.

which is taken from Milgrom and Bahcall (1978). Charged particles ejected by the central object at $O$ move relativistically along the field lines, emitting radiation in narrow cones around the tangential direction. The observer at $X$ will see only the radiation emitted in the plane determined by the dipole axis and his line-of-sight. At a given time $t_1$ after the initial ejection would have been observed, he sees radiation from two points $A(t_1)$ and $B(t_1)$ whose locations give the same total particle and radiation travel time along the paths $OAX$ and $OBX$. At a later time $t_2$, he sees radiation from two similar points $A(t_2)$ and $B(t_2)$ which are further apart than were $A(t_1)$ and $B(t_1)$. The apparent velocity of separation is superluminal for all inclination angles, having a minimum value of $4.446c$ when $\phi$ is a right angle.

For the dipole field model, the relationship between $v_T$ and the inclination angle $\phi$ has been derived by Bahcall and Milgrom (1980). If $\alpha$ and $\beta$ are, respectively, the angles from the dipole axis $d$ to the lines $OA$ and $OB$, then

$$\sin\alpha = \sqrt{\tfrac{1}{6}}[4 - \cos^2\phi - \cos\phi\sqrt{8 + \cos^2\phi}]\,, \quad 0 \le \alpha \le \sin^{-1}[\sqrt{\tfrac{2}{3}}]\,, \tag{30}$$

$$\sin\beta = \sqrt{\tfrac{1}{6}}[4 - \cos^2\phi + \cos\phi\sqrt{8 + \cos^2\phi}]\,, \quad \frac{\pi}{2} \le \beta \le \pi - \sin^{-1}[\sqrt{\tfrac{2}{3}}]\,,$$

and

$$v_T(\phi) = c\left[\frac{\sin^2\alpha\sin|\phi - \alpha|}{G(\alpha)} + \frac{\sin^2\beta\sin|\phi - \beta|}{G(\beta)}\right], \quad 0 \le \phi \le \frac{\pi}{2}\,, \tag{31}$$

where

$$G(\eta) \equiv P(\sqrt{3}) - P(\sqrt{3}\,|\cos\eta|) - \sin^2\eta\cos(\phi - \eta)\,, \tag{32}$$

with the function $P(\xi)$ being defined by

$$P(\xi) \equiv \frac{1}{2\sqrt{3}}\{\xi\sqrt{1 + \xi^2} + \ln[\xi + \sqrt{1 + \xi^2}]\}\,. \tag{33}$$

Note that although its definition is complicated, $v_T(\phi)$ is a continuous, monotonically decreasing function on the interval $[0, \pi/2]$ (see Figure 4). This means that for any given value $v^*$ of the transverse velocity, we can use a numerical equation solver to easily compute the inverse function value

$$\phi^* = v_T^{-1}(v^*)\,,$$

even though we cannot write the inverse function in a simple analytical closed form expression. Similarly, for any value $\phi^*$, we can numerically compute the derivative

$$v_T'(\phi^*) = \left.\frac{dv_T}{d\phi}\right|_{\phi=\phi^*}\,,$$

to any desired accuracy up to the limits of computer precision.

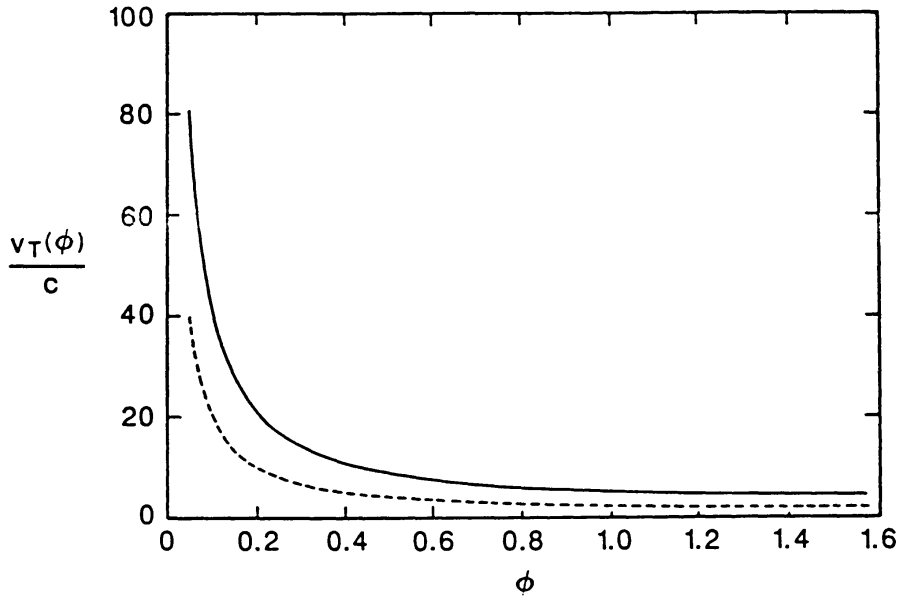


Fig. 4. Plot of the functions $v_T(\phi)/c$ for the dipole field model (solid line) and the light echo model (dashed line).

For both the light echo model and the dipole field model, the angles $\phi_1, \phi_2, \ldots, \phi_m$ should constitute a sample of size $m$ drawn from the sinusoidal probability distribution (28), but the values $\phi_i$ are not actually observed. What is observed is a sample $\dot{\theta}_1, \dot{\theta}_2, \ldots, \dot{\theta}_m$ drawn from a family of probability density functions whose form can be inferred from that of the $\phi$ distribution. Using Equation (19) we can write the random variable $\dot{\Theta}$ in terms of the random variable $\Phi$ as

$$\dot{\Theta}(z; \Phi) = \frac{v_T(\Phi)}{c} Q(z; \Lambda, H_0, q_0) . \tag{34}$$

Each of the observed $\dot{\theta}_i$ is a sample of size 1 from a probability density function $g(z_i; \dot{\theta})$ whose form is determined by the distribution for $\phi$ and the above transformation of the random variables. Using the standard procedure for making such transformations (see Hogg and Craig, 1965, Chapter 4, Section 3), it is quite straightforward to show that the required family of probability density functions can be written

$$g(z; \dot{\theta}) = \frac{c \sin\left[v_T^{-1}\left(\dfrac{c\dot{\theta}}{Q(z; \Lambda, H_0, q_0)}\right)\right]}{\left|Q(z; \Lambda, H_0, q_0) v_T'\left(v_T^{-1}\left(\dfrac{c\dot{\theta}}{Q(z; \Lambda, H_0, q_0)}\right)\right)\right|}, \quad \dot{\theta}_{\min}(z) \leq \dot{\theta} \leq \infty , \tag{35}$$

where

$$\dot{\theta}_{\min}(z) = \dot{\theta}_{\min}(z; \Lambda, H_0, q_0) = \frac{v_{\min} Q(z; \Lambda, H_0, q_0)}{c} , \tag{36}$$

and $v_T^{-1}$ and $v_T'$ are the inverse and derivative of the function $v_T(\phi)$. For the dipole field model, these two quantities must be computed numerically, but for the light echo model they can easily be written in closed form, using Equation (25), so that the above expression reduces to

$$g(z;\,\dot\theta) = \frac{4[Q(z;\,\Lambda, H_0, q_0)]^2}{\dot\theta^2\sqrt{\dot\theta^2 - 4[Q(z;\,\Lambda, H_0, q_0)]^2}}\,, \quad \dot\theta_{\min}(z) \le \dot\theta \le \infty\,. \tag{37}$$

Knowing the form of the probability density function at each measured point $(z_i,\,\dot\theta_i)$ enables us to write the likelihood function for the sample $\dot\theta_1, \dot\theta_2, \ldots, \dot\theta_m$. To simplify the notation we define an $m$-vector $\dot{\boldsymbol\theta}$ by

$$\dot{\boldsymbol\theta} = (\dot\theta_1,\,\dot\theta_2, \ldots, \dot\theta_m)^T\,. \tag{38}$$

Since each of the measured points is independent of the others, the likelihood function can be written

$$L(\dot{\boldsymbol\theta}) = \prod_{i=1}^{m} g(z_i,\,\dot\theta_i)\,.$$

Following the standard procedure (see Bard, 1974, Chapter 4, Section B), we will seek the parameter vector

$$\mathbf{x} = (\Lambda, H_0, q_0)^T \tag{39}$$

which maximizes the logarithm of this likelihood function, subject to all of the relevant constraints. This leads to a constrained maximization problem whose objective function is, by Equation (35),

$$\mathscr{F}(\mathbf{x}) = \log[L(\dot{\boldsymbol\theta})] = \sum_{i=1}^{m} \log\left\{\frac{c\,\sin\left[v_T^{-1}\left(\dfrac{c\,\dot\theta_i}{Q(z_i;\,\mathbf{x})}\right)\right]}{\left|Q(z_i;\,\mathbf{x})v_T'\left(v_T^{-1}\left(\dfrac{c\,\dot\theta_i}{Q(z_i;\,\mathbf{x})}\right)\right)\right|}\right\}. \tag{40}$$

The constraints arise from fact that the probability density functions $g(z_i,\,\dot\theta)$ are nonzero only at intervals

$$\frac{v_{\min}\,Q(z_i;\,\mathbf{x})}{c} \le \dot\theta \le \infty\,, \quad i = 1, 2, \ldots, m\,,$$

but these inequalities must be strengthened somewhat to allow for the fact that we are working with a finite sample vector $\dot{\boldsymbol\theta}$. If this were not done, then the resulting lower envelope function $\dot\theta_{\min}(z;\,\mathbf{x})$ would pass through one or more of the measured points $(z_i,\,\dot\theta_i)$, but in a finite sample, the probability of measuring a source with inclination angle exactly $\pi/2$ is zero. Therefore, we base the constraints on the expected value of the largest angle in the sample $\phi_1, \phi_2, \ldots, \phi_m$.

Let $\varphi_1$, $\varphi 2, \ldots, \varphi_m$ be the order statistics obtained by arranging the $\phi_i$ in ascending order. The probability distribution function for the largest angle $\varphi_m$ is (see Hogg and Craig, 1965, Chapter 6, Section 1)

$$f_m(\varphi_m) = m[F(\varphi_m)]^{m-1} f(\varphi_m) ,$$

where $f(\phi)$ and $F(\phi)$ are just the probability density and cumulative density functions for the angle $\phi$. Substituting Equations (28) and (29) we obtain

$$f_m(\varphi_m) = m[1 - \cos\varphi_m]^{m-1} \sin\varphi_m , \quad 0 \leq \varphi_m \leq \frac{\pi}{2} ,$$

so that, if $\phi_{\max}(m)$ is defined to be the expected value of $\varphi_m$, i.e.,

$$\phi_{\max}(m) \equiv E(\varphi_m) = \int_0^{\pi/2} \varphi_m f_m(\varphi_m)\, d\varphi_m , \tag{41}$$

then

$$\phi_{\max}(m) = \int_0^{\pi/2} \varphi_m m[1 - \cos\varphi]^{m-1} \sin\varphi\, d\varphi = \frac{\pi}{2} - \int_0^{\pi/2} [1 - \cos\varphi]^m\, d\varphi . \tag{42}$$

It is easy to see that

$$\phi_{\max}(1) = 1 , \qquad \phi_{\max}(2) = 2 - \frac{\pi}{4} ,$$

but is is tedious to show that, for $m > 2$,

$$\phi_{\max}(m) = \sum_{\nu=1}^{\nu_{\max}} \binom{m}{2\nu - 1} \frac{2^{2\nu-2}[(\nu - 1)!]^2}{(2\nu - 1)!} - \frac{\pi}{2} \sum_{\mu=1}^{\mu_{\max}} \binom{m}{2\mu} \frac{(2\mu)!}{2^{2\mu}(\mu!)^2} , \tag{43}$$

where

$$\nu_{\max} = \begin{cases} \dfrac{m}{2} , & \text{for } m \text{ even} , \\ \dfrac{m+1}{2} , & \text{for } m \text{ odd} , \end{cases} \quad \text{and} \quad \mu_{\max} = \begin{cases} \dfrac{m}{2} , & \text{for } m \text{ even} , \\ \dfrac{m-1}{2} , & \text{for } m \text{ odd} . \end{cases} \tag{44}$$

Since $\phi_{\max}(m)$ is the expected value for the largest $\phi_i$, the natural constraints for the estimation problem follow from requiring that

$$\phi_i \leq \phi_{\max}(m) , \quad i = 1, 2, \ldots, m .$$

The function $v_T(\phi)$ is a monotonically decreasing function of $\phi$, so these inequalities are satisfied only if

$$\frac{v_T(\phi_i)}{c}\, Q(z_i; \mathbf{x}) \geq \frac{v_T(\phi_{\max}(m))}{c}\, Q(z_i; \mathbf{x}), \quad i = 1, 2, \ldots, m,$$

which, by Equation (19), are the same as requiring that

$$\dot{\theta}_i \geq \frac{v_T(\phi_{\max}(\mathrm{m}))}{\mathrm{c}}\, \mathrm{Q}(\mathrm{z_i}; \mathbf{x}), \quad \mathrm{i} = 1, 2, \ldots, m. \tag{45}$$

If we define a set of constraint functions $C_i(\mathbf{x})$ by

$$C_i(\mathbf{x}) = \dot{\theta}_i - \frac{v_T(\phi_{\max}(m))}{c}\, Q(z_i; \mathbf{x}), \quad i = 1, 2, \ldots, m, \tag{46}$$

then the constraints can be written simply as

$$C_i(\mathbf{x}) \geq 0, \quad i = 1, 2, \ldots, m. \tag{47}$$

From Equation (25) it follows that the constraint functions for the light echo model are just

$$C_i(\mathbf{x}) = \dot{\theta}_i - \frac{2Q(z_i; \mathbf{x})}{\sin(\phi_{\max}(m))}, \quad i = 1, 2, \ldots, m \tag{48}$$

but for the dipole field model, they cannot be written so simply because $v_T(\phi_{\max}(m))$ must be calculated from Equations (30), (31), (32), and (33).

When the objective function (40) is maximized, subject to the constraints (47), the result is a solution vector $\mathbf{x}^*$ whose components $\Lambda^*$, $H_0^*$, and $q_0^*$ can be substituted into Equation (22) to compute the lower envelope function $\dot{\theta}_{\min}(z; \mathbf{x}^*)$. The values $\dot{\theta}_{\min}(z_i; \mathbf{x}^*)$ can then be combined with the observed $\dot{\theta}_i$ to estimate the inclination angles $\phi_i$. In the case of the light echo model, the $\phi_i$ are easily computed using Equation (26), but for the dipole field model, it is necessary to numerically invert the equations

$$\dot{\theta}_{\min}(z_i; \mathbf{x}^*) = \frac{v_T(\phi_i)}{c}\, Q(z_i; \mathbf{x}^*), \quad i = 1, 2, \ldots, m, \tag{49}$$

where the function $v_T(\phi)/c$ is the solid curve shown in Figure 4. Once the $\phi_i$ have been determined, then their estimated cumulative distribution can then be computed and compared with the predicted distribution (29) to check whether the observed data are consistent with the combination of the assumed source model and the Friedmann cosmology specified by the parameter estimates $\Lambda^*$, $H_0^*$, and $q_0^*$.

## 4. Numerical Analysis

The constrained estimation problem which must be solved to find the maximum likelihood estimates for the parameters **x** can be written

$$\mathscr{L}_{\min} = \min_{\mathbf{x}} \{\mathscr{L}(\mathbf{x}) : C_i(\mathbf{x}) \geq 0, i = 1, 2, \ldots, m\}, \tag{50}$$

where the $C_i(\mathbf{x})$ are defined by Equations (46), and

$$\mathscr{L}(\mathbf{x}) = -\mathscr{F}(\mathbf{x}), \tag{51}$$

with $\mathscr{F}(\mathbf{x})$ given by Equation (40). Its solution is not a trivial calculation, even in the two-parameter case obtained by assuming $\Lambda = 0$. Fortunately, it can be solved by the off-the-shelf subroutine E04VBF from the NAg Library (see Numerical Algorithms Group, 1984, Vol. 3). The algorithm, which has been described in Gill and Murray (1974) and by Murray (1976), uses a sequential augmented Lagrangian method, solving the minimization subproblems by a modified Newton method.

Subroutine E04VBF requires three user-supplied subroutines: FUNCT2, CON2, and AMONIT. The latter allows the user to specify printing of intermediate results in order to monitor the optimization iteration. During the iteration E04VBF calls FUNCT2 with estimates of the parameters **x** and the latter must return the corresponding values of the objective function and its first derivatives with respect to those parameters. Similarly subroutine CON2 must return the current values of the constraint functions and their derivatives with respect to **x**. We wrote these subroutines to use either the light echo model or the dipole field model, and for each model to accomodate both the two parameter case where it is assumed that $\Lambda = 0$ and the three parameter case where $\Lambda$ is a parameter to be determined. In the following we will denote the number of parameters by $n$, i.e.,

$$n = 2 \Rightarrow \mathbf{x} = (H_0, q_0)^T, \quad \Lambda \equiv 0,$$

$$n = 3 \Rightarrow \mathbf{x} = (\Lambda, H_0, q_0)^T.$$

Subroutines FUNCT2 and CON2 connect E04VBF to a network of other subroutines and function subprograms required to provide the necessary function values and derivatives. This subroutine hierarchy is illustrated in Figure 5. Subroutine FUNCT2 calls FCALC to calculate the objective function

$$\mathscr{L}(\mathbf{x}) = -\sum_{i=1}^{m} \log \left\{ \frac{c \sin\left[ v_T^{-1}\left( \frac{c\dot{\theta}_i}{Q(z_i;\mathbf{x})} \right) \right]}{\left| Q(z_i;\mathbf{x}) v_T'\left( v_T^{-1}\left( \frac{c\dot{\theta}_i}{Q(z_i;\mathbf{x})} \right) \right) \right|} \right\}. \tag{52}$$

For the light echo model, this reduces to

$$\mathscr{L}(\mathbf{x}) = -\sum_{i=1}^{m} \log \left\{ \frac{4[Q(z_i;\mathbf{x})]^2}{\dot{\theta}_i^2 \sqrt{\dot{\theta}_i^2 - 4[Q(z_i;\mathbf{x})]^2}} \right\}. \tag{53}$$

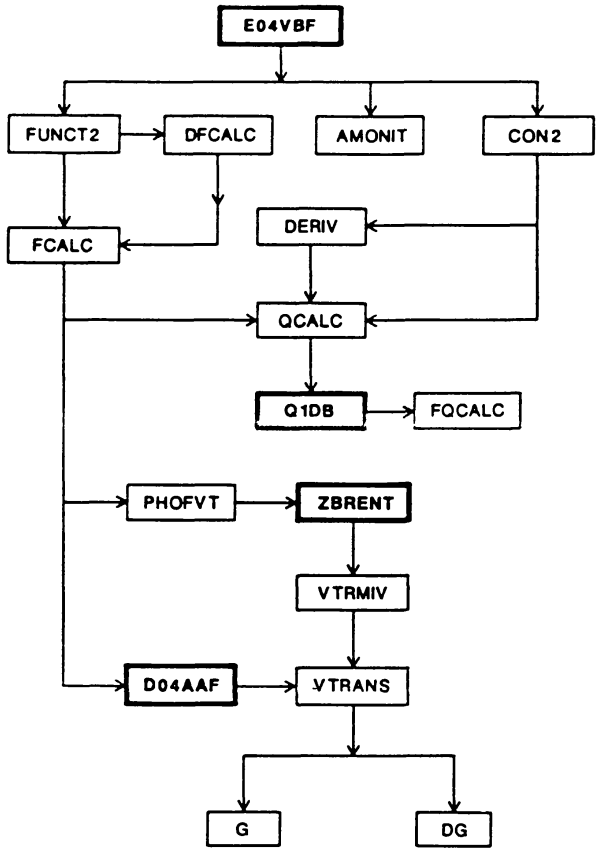


Fig. 5. The E04VBF subroutine hierarchy. Bold-faced boxes indicate off-the-shelf subroutines. The other subroutines were written by the present authors.

Note that this objective function is not defined for parameter vectors $\mathbf{x}$ such that

$$\dot{\theta}_i \leq 2Q(z_i; \mathbf{x}), \quad \text{for any } z_i,$$

but this is of no concern so long as the constraints are not violated. For the light echo model the constraints are just

$$\dot{\theta}_i - \frac{2Q(z_i; \mathbf{x})}{\sin(\phi_{\max}(m))} \geq 0, \quad i = 1, 2, \ldots, m,$$

and, for any finite sample size, $\sin(\phi_{\max}(m))$ is strictly less than unity, so there is a buffer zone in the parameter space between the limits of the feasible region and the boundary on which objective function blows up.

The situation in the case of the dipole field model is exactly the same, but there is no way to simplify the expression (52) for the objective function. We can rewrite it in the form

$$\mathscr{L}(\mathbf{x}) = -\sum_{i=1}^{m} \log \left\{ \frac{\sin\left[ V_T^{-1}\left( \frac{\dot{\theta}_i}{Q(z_i; \mathbf{x})} \right) \right]}{\left| Q(z_i; \mathbf{x}) V_T'\left( V_T^{-1}\left( \frac{\dot{\theta}_i}{Q(z_i; \mathbf{x})} \right) \right) \right|} \right\}, \tag{54}$$

where

$$V_T(\phi) \equiv \frac{v_T(\phi)}{c} , \tag{55}$$

but in order to calculate it, the function $V_T(\phi)$, shown as the solid curve in Figure 4, must be inverted and differentiated numerically. For each given velocity ratio

$$V_i = \frac{\dot{\theta}_i}{Q(z_i; \mathbf{x})} ,$$

FCALC calls subroutine PHOFVT to compute the required $\phi_i$, i.e.,

$$\phi_i = V_T^{-1}(V_i) .$$

PHOFVT is simply an interface which calls the IMSL subroutine ZBRENT to calculate the zero of the function $V_T(\phi) - V_i$, i.e., to solve the equation

$$V_T(\phi) - V_i = 0 ,$$

(see IMSL User's Manual, 1984, Vol. 4). The above equation is guaranteed to have exactly one solution so long as none of the constraints are violated. ZBRENT uses the algorithm of Brent (1971) which combines linear interpolation, inverse quadratic interpolation, and interval bisection to iterate from the user's initial guess to an estimate guaranteed to be within a user-specified tolerance of the zero. It requires that the user provide a real function subprogram which, for a given iterate $\hat{\phi}$, returns the function value $V_T(\hat{\phi}) - V_i$. This is accomplished by function VTRMIV which in turn calls a function subprogram VTRANS to compute $V_T(\hat{\phi})$. The latter value is computed using Equations (30), (31), (32), and (33). It should be noted that the evaluation of $G(\eta)$ by Equation (32) is very sensitive to cancellation errors for small values of $\eta$. Accordingly function VTRANS calls a single precision real function subprogram $G$ to make the calculation for larger values of $\eta$ and a double precision variant $DG$ for smaller values.

In order to compute the derivatives $V_T'(\phi_i)$, FCALC calls the NAg subroutine D04AAF (Numerical Algorithms Group, 1984, Vol. 2) which uses an extension of the Neville algorithm. The method has been described by Lyness and Moler (1966, 1969). D04AAF requires the user to provide a real function subprogram to evaluate the function $V_T(\phi)$ for various values of $\phi$. To do this, we used the function subprogram VTRANS described in the preceding paragraph.

For both the light echo and the dipole field models, the calculation of the objective function $\mathscr{L}(\mathbf{x})$ for a given set of parameter iterates $\hat{\mathbf{x}}$ requires the evaluation of the quantities $Q(z_i; \hat{\mathbf{x}})$, $i = 1, 2, \ldots, m$. FCALC obtains these values by calling subroutine QCALC. For $n = 2$ they are defined by

$$Q(z_i; \hat{\mathbf{x}}) = \frac{\hat{H}_0 \hat{q}_0^2 (1 + z_i)}{\hat{q}_0 z_i + (\hat{q}_0 - 1)(-1 + \sqrt{2\hat{q}_0 z_i + 1})} , \tag{56}$$

but, in the interest of numerical stability, QCALC evaluates the equivalent expressions

$$Q(z_i; \hat{\mathbf{x}}) = \frac{\hat{H}_0(z_i + 1)\,[\sqrt{1 + 2\hat{q}_0 z_i} + 1]^2}{2z_i[\sqrt{1 + 2\hat{q}_0 z_i} + z_i + 1]} \,. \tag{57}$$

For $n = 3$ the situation is much more complicated, with the $Q(z_i, \hat{\mathbf{x}})$ being defined by Equations (20) and (21). In order to compute the integrals $I(z_i; \hat{\mathbf{x}})$ defined by (21), QCALC calls the numerical quadrature subroutine Q1DB from the National Bureau of Standards GAMS library (Boisvert *et al.*, 1984). Q1DB uses an adaptive quadrature algorithm (Kahaner *et al.*, 1989, Chapt. 5) which automatically adjusts the mesh size to obtain the accuracy specified by the user, and in the adjustment process attempts to minimize the amount of work required to obtain that accuracy. This is an important consideration because these integral calculations are repeated many times during the optimization iteration. In evaluating the integrals Q1DB calls the user-supplied function subprogram FQCALC to compute the integrand at each mesh point. FQCALC was coded to minimize the number of multiplications required to evaluate the quartic polynomial, using the nested form

$$\left\{\left[\frac{\hat{\Lambda}}{3}\,\xi^2 + (\hat{H}_0^2 - 2\hat{q}_0\hat{H}_0^2 - \hat{\Lambda})\right]\xi + \left[2\hat{q}_0\hat{H}_0^2 + 2\,\frac{\hat{\Lambda}}{3}\right]\right\}\xi \,,$$

and ordering the calculation of the coefficients as efficiently as possible.

Subroutine FUNCT2 is also required to provide E04VBF with the partial derivatives of $\mathscr{L}(\mathbf{x})$ with respect to the parameters $\mathbf{x}$ evaluated at the iterate values $\hat{\mathbf{x}}$. For $n = 2$ and the light echo model it is possible, but extremely messy, to find algebraic closed form expressions for these derivatives, but for all other cases, this is not possible. Therefore, in all cases the derivatives are computed numerically in subroutine DFCALC which uses the central differencing approximations

$$\frac{\partial \mathscr{L}(\hat{\mathbf{x}})}{\partial x_j} = \frac{\mathscr{L}(\hat{\mathbf{x}} + \Delta x_j \mathbf{e}_j) - \mathscr{L}(\hat{\mathbf{x}} - \Delta x_j \mathbf{e}_j)}{2\Delta x_j} \,, \quad j = 1, \ldots, n \,,$$

where $\mathbf{e}_j$ denotes the unit vector with a 1 for the $j$th component. DFCALC calls subroutine FCALC to obtain the values $\mathscr{L}(\hat{\mathbf{x}} \pm \Delta x_j \mathbf{e}_j)$.

Subroutine E04VBF calls the user-supplied subroutine CON2 to evaluate the constraint functions and their derivatives with respect to the parameters. The constraints are easily calculated by evaluating Equations (46) for the iterate $\hat{\mathbf{x}}$ with calls to subroutine QCALC to obtain the values $Q(z_i; \hat{\mathbf{x}})$. The quantity

$$V_T(\phi_{\max}(m)) = \frac{v_T(\phi_{\max}(m))}{c}$$

is calculated once only, at the very beginning of the main program, before the call to E04VBF. It is calculated by calling the function subprogram VTRANS (described in the preceding) with the argument $\phi = \phi_{\max}(m)$. The value of $\phi_{\max}(m)$ is calculated from

Equation (42), with a call to the quadrature subroutine Q1DB, described above, to evaluate the integral

$$\int_0^{\pi/2} [1 - \cos\varphi]^m \, d\varphi \, .$$

Although this integration can be carried out analytically, resulting in the closed form expression (43) for $\phi_{\max}(m)$, the actual finite precision computer calculation by this method is unstable for larger values of $m$. On the Cyber 855, whose single precision floating point numbers have 14 significant digitis, this breakdown occurs at $m = 38$.

From Equations (46) it follows that the partial derivatives of the constraint functions with respect to the parameters are given by

$$\frac{\partial C_i(\hat{\mathbf{x}})}{\partial x_j} = -\frac{v_T(\phi_{\max}(m))}{c} \frac{\partial Q(z_i; \hat{\mathbf{x}})}{\partial x_j} \, , \quad i = 1, 2, \ldots, m \, , \quad j = 1, \ldots, n \, .$$

CON2 calls subroutine DERIV to compute the partial derivatives of the $Q(z_i; \mathbf{x})$ with respect to the $x_j$. For the $n = 2$ case, DERIV calculates

$$\frac{\partial Q(z_i; \hat{\mathbf{x}})}{\partial H_0} = \frac{(z_i + 1)\,[\sqrt{1 + 2\hat{q}_0 z_i} + 1]^2}{2x_i[\sqrt{1 + 2\hat{q}_0 z_i} + z_i + 1]} \, ,$$

$$\frac{\partial Q(z_i; \hat{\mathbf{x}})}{\partial q_0} = \frac{\hat{H}_0(z_i + 1)\,[\sqrt{1 + 2\hat{q}_0 z_i} + 1]\,[\sqrt{1 + 2\hat{q}_0 z_i} + 2z_i + 1]}{2[\sqrt{1 + 2\hat{q}_0 z_i} + z_i + 1]^2 \sqrt{1 + 2\hat{q}_0 z_i}} \, ,$$

which are obtained by differentiating Equation (57). For $n = 3$ the $Q(z_i; \mathbf{x})$ are too complicated for this direct approach so DERIV calculates the derivatives by the central differencing approximations

$$\frac{\partial Q(z_i; \hat{\mathbf{x}})}{\partial x_j} \doteq \frac{Q(z_i; \hat{\mathbf{x}} + \Delta x_j \mathbf{e}_j) - Q(z_i; \hat{\mathbf{x}} - \Delta x_j \mathbf{e}_j)}{2\Delta x_j} \, ,$$

$$i = 1, 2, \ldots, m \, , \quad j = 1, 2, 3 \, ,$$

calling subroutine QCALC to obtain the values $Q(z_i; \hat{\mathbf{x}} \pm \Delta x_j \mathbf{e}_j)$.

## 5. Analysis of Yahil's Simulated Data Set

In order to validate our statistical and numerical procedures, we applied our analysis to Yahil's simulated data set (Figure 1) using $n = 2$ (assuming $\Lambda = 0$). Yahil did not tabulate these data, so that we had to read them from the graph in his paper (Yahil, 1979, Figure 1). The digitizing errors thus incurred are probably considerably smaller than the typical measurement errors for the $\dot{\theta}$ and not too much larger than the typical measurement errors for the $z$. We ran the program using both the light echo and

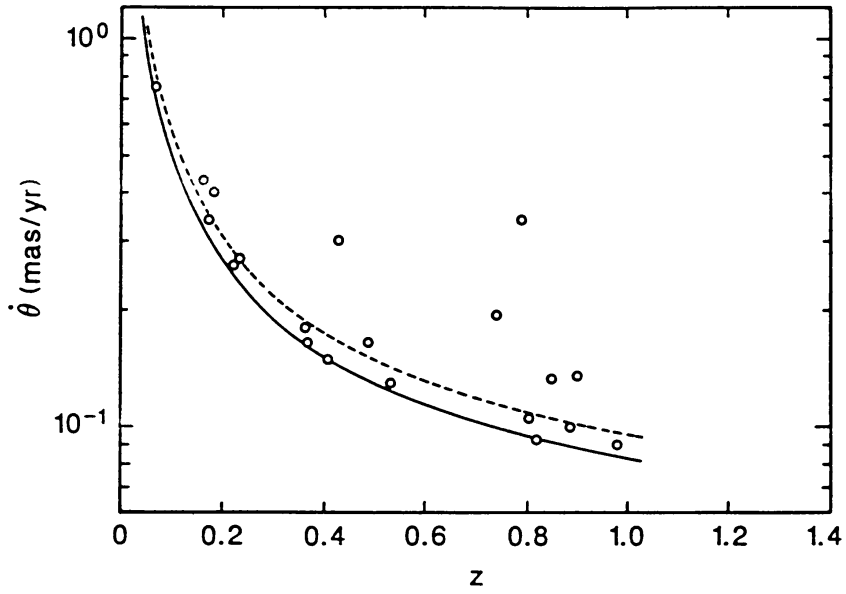


Fig. 6. The $n = 2$ lower envelope fit to Yahil's simulated data set. The dashed curve is the estimated median locus.

the dipole field source models. The two models produced fitted envelope curves that are identical to the limits of graphical accuracy. This common curve is shown in Figure 6 which also shows the expected median curve. The latter is easily obtained by observing that the median for the sinusoidal distribution (28) is

$$\phi_{\text{med}} = \frac{\pi}{3} ,$$

so the median locus for $\dot{\theta}$ is defined by

$$\dot{\theta}_{\text{med}}(z) = \frac{v_T(\pi/3)}{c} \, Q(z; \mathbf{x}) , \tag{58}$$

where $\mathbf{x}$ is the vector of parameter values determined by the fit. For the light echo model, the above expression reduces to

$$\dot{\theta}_{\text{med}}(z) = \frac{4}{\sqrt{3}} \, Q(z; \mathbf{x}) ,$$

but for the dipole field model, the value $v_T(\pi/3)/c$ must be computed from Equations (30)–(33), using the function subprogram VTRANS described in the preceding section. In spite of this difference the two median curves thus obtained are identical to graphical accuracy.

The parameter estimates obtained for the fits are given in Table I which lists the Hubble constant $H$ in units of (km s$^{-1}$ Mpc$^{-1}$) rather than the $H_0$ values actually

TABLE I
Parameter estimates for Yahil's simulated data set

| Source model | $H$ | $q_0$ |
|---|---|---|
| Light echo | 109.7 | 0.62 |
| Dipole field | 49.4 | 0.62 |

calculated by the program. The parameters determined for the dipole field model compare favourably with the values $H = 50.0$ and $q_0 = 0.5$ used by Yahil to generate the data. He anticipated that the data would determine $q_0$ to an accuracy $\Delta q_0 \sim 0.1$, and the difference between his assumed value and the value actually determined by the fit is not inconsistent with that expectation. This difference would no doubt have been smaller if his sample had extended to larger red shifts. The value obtained for $q_0$ with the light echo model was essentially the same as that obtained with the dipole field model. They differed only by 8 units in the fourth significant figure. Also, the light echo value of $H$ is larger than the dipole field value by a factor of 2.223 which is exactly the inverse of the ratio of minimum velocities for the two models.

As explained in Section 3, the determination of the lower envelope curve yields estimates for the inclination angles for the individual sources. For a sample of randomly oriented sources, the cumulative distribution for these angles should approximate the theoretical distribution (29). In Figure 7 the theoretical distribution is plotted as a

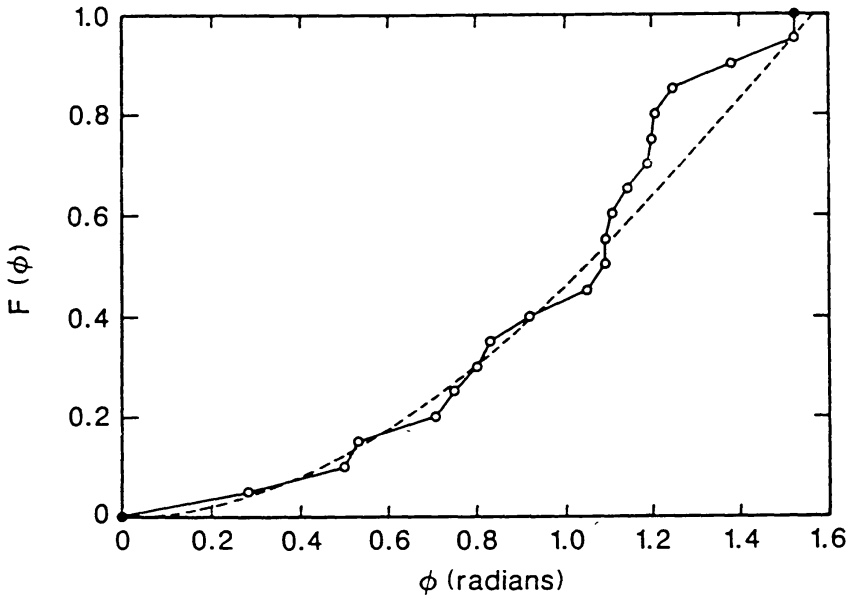


Fig. 7. Comparison of the estimated cumulative distribution of inclination angles in Yahil's simulated data set with the distribution expected for randomly oriented sources. The dashed curve is the expected distribution and the discrete points connected by line segments represent the estimated distribution.

dashed line and the cumulative distribution for the sample is plotted as discrete points connected by solid line segments. The good agreement between these two distributions suggests not only that Yahil generated a truly randomly oriented sample, but also that our estimation procedures treated the data correctly.

## 6. A Real Data Set

There are now more than thirty known radio sources exhibiting superluminal expansion, and the number observed is growing so rapidly that any compilation of their expansion rates is soon out of date. The measured data used in this study are given in Table II. These data were taken for the most part from a list compiled by Zensus and Pearson

TABLE II

Measured angular separation rates for 'superluminal' radio sources

| $z$ | $\dot{\theta}$ | Source | $z$ | $\dot{\theta}$ | Source | $z$ | $\dot{\theta}$ | Source |
|---|---|---|---|---|---|---|---|---|
| 0.033 | 1.35 | 3C120 | 0.424 | 0.18 | 0735 + 178 | 0.846 | 0.19 | 3C179 |
| 0.033 | 2.55 | 3C120 | 0.538 | 0.5 | 3C279 | 0.851 | 1.34 | 0235 + 164 |
| 0.0695 | 0.76 | BL Lac | 0.538 | 0.11 | 3C279 | 0.859 | 0.35 | 3C454.3 |
| 0.158 | 0.775 | 3C273 | 0.595 | 0.48 | 3C345 | 1.029 | 0.11 | 3C245 |
| 0.158 | 0.99 | 3C273 | 0.595 | 0.30 | 3C345 | 1.037 | 0.65 | CTA 102 |
| 0.158 | 1.20 | 3C273 | 0.635 | 0.64 | 3C395 | 1.25 | 0.13 | 1150 + 812 |
| 0.206 | 0.36 | 4C34.47 | 0.669 | 0.11 | 3C216 | 1.258 | 0.15 | NRAO 140 |
| 0.302 | 0.6 | 1928 + 738 | 0.699 | 0.16 | 4C39.25 | 1.322 | 0.12 | 0850 + 581 |
| 0.306 | 0.28 | OJ 287 | 0.751 | 0.34 | 1642 + 690 | 2.367 | 0.09 | 0212 + 735 |

for the IAU Symposium No. 129 (see Zensus and Pearson, 1988, Table 1). We made the following alterations in that list:

(1) Two sources, with estimated apparent velocities $1.2c$ and $1.3c$, were deleted from the list.

(2) For multicomponent sources, components having nearly equal measured $\dot{\theta}$-values were combined to give one data point.

(3) We added one additional source (0235 + 164) (see Scheuer, 1976; and Bååth, 1984).

We removed the two sources 3C263 and 1951 + 498 because their apparent linear expansion rates were too small to be consistent with either of the source models used in the study. It is possible that they could be one-sided light echoes, i.e., stationary sources exciting a light echo in only one direction. We eliminated these sources before attempting to do any fits and believe that our criterion is valid. There is no good reason to believe that all observed apparent superluminal velocities are caused by the same mechanism. In fact, the results of the fits strongly suggest that such is not the case. For the multicomponent sources, it seems likely that components with nearly equal $\dot{\theta}$-values represent a common inclination angle. Thus they were averaged rather than counted separately in order not to spoil the angular distribution statistics. Components

with distinctly different $\dot{\theta}$-values were counted separately because they must represent different inclination angles. To support these conventions we note that SS433 is an example of a source, albeit subluminal, in which components are ejected at angles well known from precession rates, but there are instances, however, when for some unknown reason, ejecta are emitted at unpredictable angles (Romney *et al.*, 1987).

## 7. Analysis of the Real Data Set

We applied our analysis to the real data set using both the two-parameter cosmological model (24) and the three parameter model defined by (20), (21), and (22). In each case we ran the program using both the light echo and the dipole field source models. In each case the two source models gave the same lower envelope and median curves to graphical accuracy.

The fits for the two parameter case are shown in Figure 8, and the parameter estimates are given in Table III. The Hubble constant is given in the usual units (km $s^{-1}$ $Mpc^{-1}$)

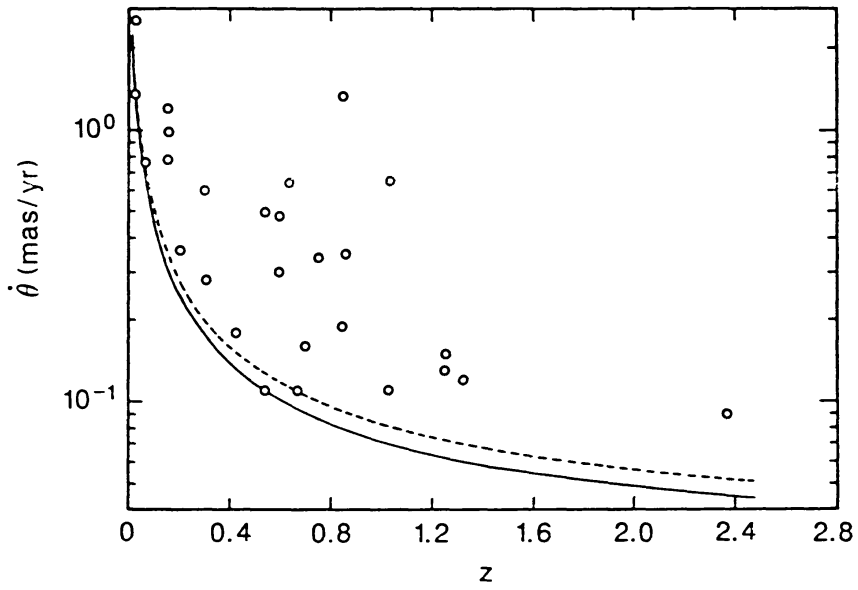


Fig. 8. The $n = 2$ lower envelope fit to the Zensus–Pearson data set. The dashed curve is the estimated median locus.

TABLE III

Parameter estimates for the two parameter cosmological model

| Source model | $H$ | $q_0$ | $\Omega_0$ | Age (yr) |
|---|---|---|---|---|
| Light echo | 103.1 | 0.41 | 0.82 | $6.6 \times 10^9$ |
| Dipole field | 46.4 | 0.41 | 0.82 | $15 \times 10^9$ |

rather than in the units used for $H_0$ by the fitting program. The two values of $q_0$ differed by only 8 units in the fourth significant digit, and the ratio of the two $H_0$ estimates was 2.224 which is very close to the inverse ratio of the corresponding minimum velocities for the two models. Note that the light echo estimate for $H$ is consistent with the value $H = 110 \pm 10$ obtained by Lynden-Bell (1977) who used only the single source 3C120. The table also includes the estimate of the density parameter $\Omega_0$, which for the $n = 2$ cosmological model is just

$$\Omega_0 = 2q_0 ,$$

and very rough estimates ($0.75H^{-1}$) of the corresponding age of the Universe obtained from the very useful graphs given by Felten and Isaacman (1986). For both source models the estimated universe is open and will expand forever, but when one considers the magnitude of the error in the $q_0$ estimates for Yahil's simulated data set, it is obvious that a closed universe cannot be ruled out with any confidence.

Although the cosmological parameter estimates in Table III are quite reasonable and consistent with results currently obtained by other methods, it is very obvious from a cursory inspection of Figure 8 that the distribution of the measured data points is not consistent with the assumptions used in the analysis. Almost all of the measured points fall above the estimated median locus! This point is even more dramatically emphasized by Figure 9 which gives the cumulative distribution function for the inclination angles.

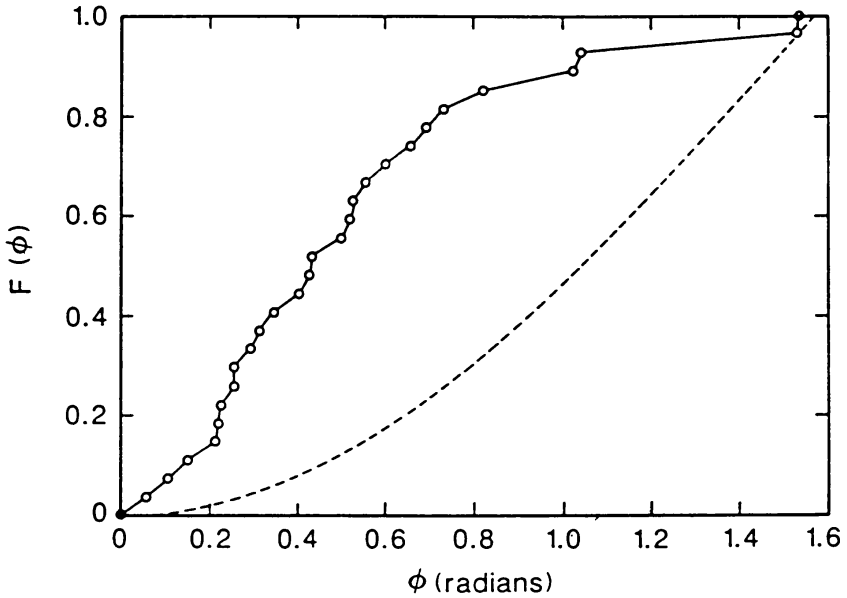


Fig. 9. Comparison of the two-parameter, estimated cumulative distribution of inclination angles with the distribution expected for randomly oriented sources. The dashed curve is the expected distribution and the discrete points connected by line segments represent the estimated distribution.

A comparison with Figure 7 leaves no doubt that the present sample does not satisfy some or all of the assumptions. We will try to address this problem in the next section.

There are not yet enough data at higher redshifts to really justify the addition of the third parameter $\Lambda$ to the cosmological model, but we carried out the exercise in order to get some indication about whether or not it will become profitable to do so when more data become available. The resulting fits, which were graphically identical, are shown in Figure 10 and the parameter estimates are given in Table IV. The value of $\Lambda$ is given in terms of $H_0^2$ and the density parameter was computed from

$$\Omega_0 = 2q_0 - \frac{2}{3}\left(\frac{\Lambda}{H_0^2}\right).$$

The age estimate ($0.5H^{-1}$) was determined from the graphs of Felten and Isaacman (1986). The fits correspond to a closed universe that will expand forever, but no

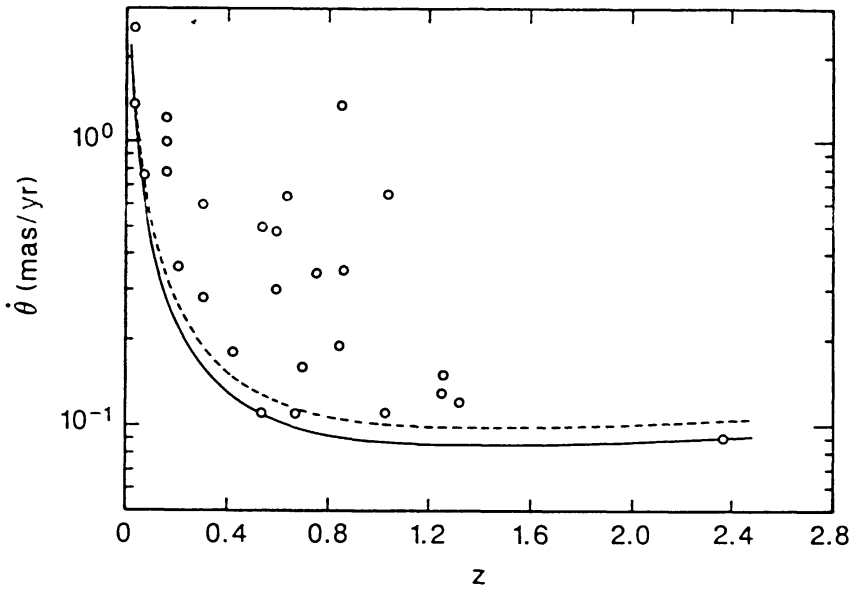


Fig. 10. The $n = 3$ lower envelope fit to the Zensus–Pearson data set. The dashed curve is the estimated median locus.

TABLE IV

Parameter estimates for the three parameter cosmological model

| Source model | $H$ | $q_0$ | $\Lambda/H_0^2$ | $\Omega_0$ | Age (yr) |
|---|---|---|---|---|---|
| Light echo | 105 | −1.0 | 6.7 | 2.5 | $4.5 \times 10^9$ |
| Dipole field | 47 | −1.0 | 6.7 | 2.5 | $10 \times 10^9$ |

confidence at all can be attached to this result since it was largely determined by the single source 0212 + 735 at redshift $z = 2.367$. The fit does indicate that Yahil was probably right in his conjecture that, given sufficient data, the method could determine

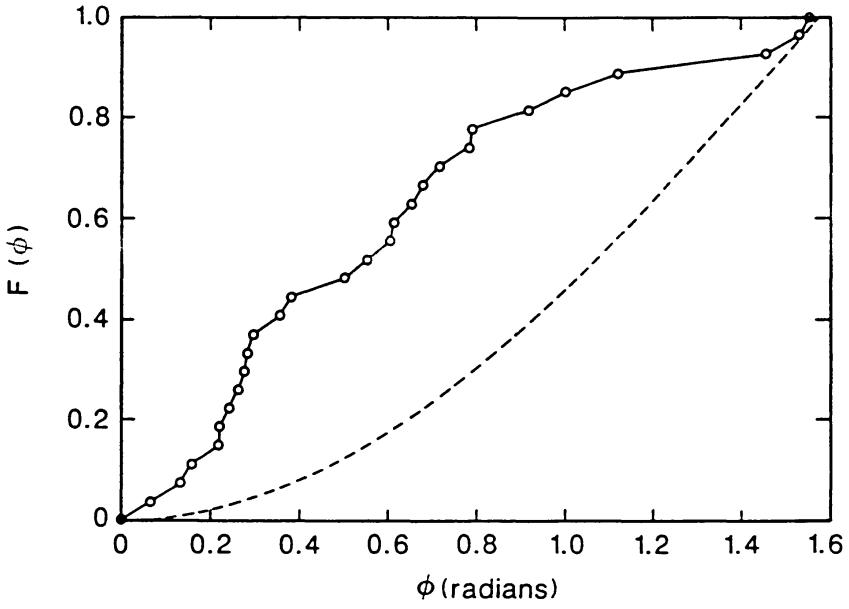


Fig. 11. Comparison of the three-parameter, estimated cumulative distribution of inclination angles with the distribution expected for randomly oriented sources. The dashed curve is the expected distribution and the discrete points connected by line segments represent the estimated distribution.

$\Lambda$. The cumulative distribution of the inclination angles is given in Figure 11. Clearly the addition of the extra parameter does little to alleviate the discrepancy between the actual and expected distributions.

## 8. Discussion and Conclusions

This study has shown that if a Friedmann cosmology is the correct model for the Universe, and if the superluminal radio sources are correctly described by a model which predicts a sharp lower bound for their apparent transverse velocities, then Yahil's suggestion for fitting a lower envelope curve to the measured data points does indeed provide a powerful method for estimating the cosmological parameters $H$, $q_0$, and $\Lambda$. Using the measurements currently available and assuming $\Lambda = 0$ gives

$$H \approx \begin{cases} 103\ (\text{km s}^{-1}\ \text{Mpc}^{-1}), & \text{if the light echo model is correct,} \\ 46\ (\text{km s}^{-1}\ \text{Mpc}^{-1}), & \text{if the dipole field model is correct.} \end{cases}$$

Thus, verification of either of the two source models would settle the current controvrsy about the distance scale. Both source models give

$$q_0 \approx 0.4\,,$$

which implies an open universe, but the uncertainty in this result is still too large to rule out the possibility that $q_0 > 0.5$. There also remains the possibility that $\Lambda \neq 0$, but it appears that the method can be used for determining $\Lambda$ if expansion velocities can be measured for more sources at higher redshifts.

All of the above conclusions are subject to a very large caveat. *The distribution of inclination angles inferred from the fitted lower envelope is totally inconsistent with the one that would be generated by a sample of randomly oriented sources.* Proponents of other source models will probably use this fact to argue that neither the light echo nor the dipole field model is correct. The fact remains, however, that both of them give reasonable parameter estimates, consistent with those obtained by other methods applied to other kinds of data. It is also almost certain that there is a strong selection effect in the sample. Higher expansion rates, which correspond to smaller inclination angles, will naturally be measured more readily than lower rates. The important question here is whether, after a decade of measuring these sources, this selection effect is strong enough to account for the observed discrepancy.

Another possibility that should be considered is that the sample is a mixture of different kinds of sources. For example, a sample contaminated with relativistic beaming sources would produce a real excess of low inclination angles which is just what we observe. The kinetic equations describing the time delay effect for the beam models are similar to the ones for the light echo model. The main difference is that for the beam models, the beams radiate only into a narrow cone centered on the direction of motion. Thus, the only beam sources that could be observed would be those at small inclinations.

Another possibility is that a mixture of light echo and dipole field sources, interpreted as all light echo, would produce the appearance of an excess of sources with low inclination angles. It might be possible to play statistical games with the data in an attempt to explain the observed distribution of inferred inclinations in terms of some such mixture, together with selection effects, but real progress in this direction requires some independent (preferably observational) means for distinguishing between the different kinds of sources.

Finally, there is one more possibility that should be considered. The Friedmann cosmological models may be wrong. At this time we cannot simply ignore Segal's chronometric cosmology which has previously been used to explain the observations in terms of subluminal velocities (Segal, 1979). It should be noted also, that the chronometric cosmology is not, in itself, inconsistent with apparent superluminal motions arising from light echo or dipole field sources. It predicts a lower envelope curve defined by

$$\dot{\theta} = \frac{v_{\min}}{c} \frac{1+z}{2R\sqrt{z}} ,$$

which has the right shape to fit the observed data with only one adjustable parameter $R$, the 'radius' of the Universe. Fitting this envelope to the Zensus–Pearson data set gives $R \approx 1540$ Mpc for the light echo model and $R \approx 3420$ Mpc for the dipole field model. In his subluminal interpretation, Segal used $R = 60$ Mpc which is more consistent with other kinds of observed data.

The steady state cosmology also predicts a one parameter envelope

$$\dot{\theta} = \frac{v_{\min}}{c} \frac{H_0}{z} .$$

If this envelope is fitted to the data, the result is $H \approx 106$ km s$^{-1}$ Mpc$^{-1}$ for the light echo model and $H \approx 47$ km s$^{-1}$ Mpc$^{-1}$ for the dipole field model. Thus, the fits shown in Figure 8 should not be interpreted as evidence for the correctness of the Friedmann cosmology.

If the Friedmann models are correct, and if one of the two source models used here can be independently verified, then Yahil's method will indeed become a powerful tool for estimating the cosmological parameters once more observations become available. Specifically what are needed are measurements of superluminal motions at higher redshifts in order to better determine $q_0$ and $\Lambda$. We also respectfully suggest more VLBI observations on the currently known sources in order to determine the $\dot{\theta}$ more precisely and to get estimates of the probable errors in these measured values. Such estimates are needed in order to determine the sensitivities of the parameters to measurement errors.

## Acknowledgements

The authors gratefully acknowledge the advice and encouragement received from Drs R. F. Boisvert, J. E. Felten, M. A. Greene, D. K. Kahaner, and D. P. O'Leary.

## References

Bååth, L. B.: 1984, 'VLBI and Compact Radio Sources', in R. Fanti, K. Kellerman, and G. Setti (eds.), *IAU Symp.* **110**, 127.
Bahcall, J. N. and Milgrom, M.: 1980, *Astrophys. J.* **236**, 24.
Bard, Yonathan: 1974, *Nonlinear Parameter Estimation*, Academic Press, New York.
Boisvert, R. F., Howe, S. E., and Kahaner, D. K.: 1984, *The Guide to Available Mathematical Software (GAMS)*, PB 84-171305, National Technical Information Service, Springfield, VA.
Brent, R. P.: 1971, *The Computer J.* **14**(4), 422.
De Waard, G. J.: 1986, 'Thermal-Nonthermal Relationships in Active Galactic Nuclei', Ph.D. thesis, Rijksuniversiteit Leiden.
Felten, J. E. and Isaacman, R.: 1986, *Rev. Mod. Phys.* **58**, 689.
Gill, P. E. and Murray, W. (ed.): 1974, *Numerical Methods for Constrained Minimization*, Academic Press, New York.
Hogg, R. V. and Craig, A. T.: 1965, *Introduction to Mathematical Statistics*, Macmillan, New York.
IMSL User's Manual: 1984, *The IMSL Library: FORTRAN Subroutines for Mathematics and Statistics*, International Mathematical and Statistical Libraries, Inc., Houston.
Kahaner, D. K., Moler, C. B., and Nash, S. G.: 1989, *Numerical Methods and Software*, Prentice-Hall, Inc., Englewood Cliffs.
Lynden-Bell, D.: 1977, *Nature* **270**, 396.
Lyness, J. N. and Moler, C. B.: 1966, *Numer. Math.* **8**, 458.
Lyness, J. N. and Moler, C. B.: 1969, *Numer. Math.* **14**, 1.
McVittie, G. C.: 1965, *General Relativity and Cosmology*, Univ. of Illinois Press, Urbana.
Milgrom, M. and Bahcall, J. N.: 1978, *Nature* **274**, 349.
Murray, W.: 1976, 'Methods for Constrained Optimization', in L. C. W. Dixon (ed.), *Optimization in Action*, Academic Press, New York.
Numerical Algorithms Group 1984, *NAg FORTRAN Library Manual Mark 11*, Numerical Algorithms Group, Oxford.
Rees, M. J.: 1966, *Nature* **211**, 468.
Romney, J. D., Schilizzi, R. T., Fejas, I., and Spencer, R. E.: 1987, *Astrophys. J.* **321**, 822.

Sanders, R. H.: 1974, *Nature* **248**, 390.
Scheuer, P. A. G.: 1976, *Monthly Notices Roy. Astron. Soc.* **177**, 1P.
Scheuer, P. A. G.: 1984, 'VLBI and Compact Radio Sources', in R. Fanti, K. Kellermann, and G. Setti (eds.), *IAU Symp.* **110**, 197.
Segal, I. E.: 1979, *Astrophys. J.* **227**, 15.
Weinberg, S.: 1972, *Gravitation and Cosmology*, Wiley, New York.
Yahil, A.: 1979, *Astrophys. J.* **233**, 775.
Zensus, J. A. and Pearson, T. J.: 1988, 'Superluminal Radio Sources', in J. Moiran and M. Reid (eds.), *Proc. IAU Symp.* **129**.